Science Advances
AAAS

advances.sciencemag.org/cgi/content/full/5/3/eaav6322/DC1

Supplementary Materials for

Hybrid nanocarriers incorporating mechanistically distinct drugs for lymphatic CD4$^+$ T cell activation and HIV-1 latency reversal

Shijie Cao, Sarah D. Slack, Claire N. Levy, Sean M. Hughes, Yonghou Jiang, Christopher Yogodzinski, Pavitra Roychoudhury, Keith R. Jerome, Joshua T. Schiffer, Florian Hladik, Kim A. Woodrow*

*Corresponding author. Email: woodrow@uw.edu

Published 27 March 2019, *Sci. Adv.* **5**, eaav6322 (2019)
DOI: 10.1126/sciadv.aav6322

This PDF file includes:

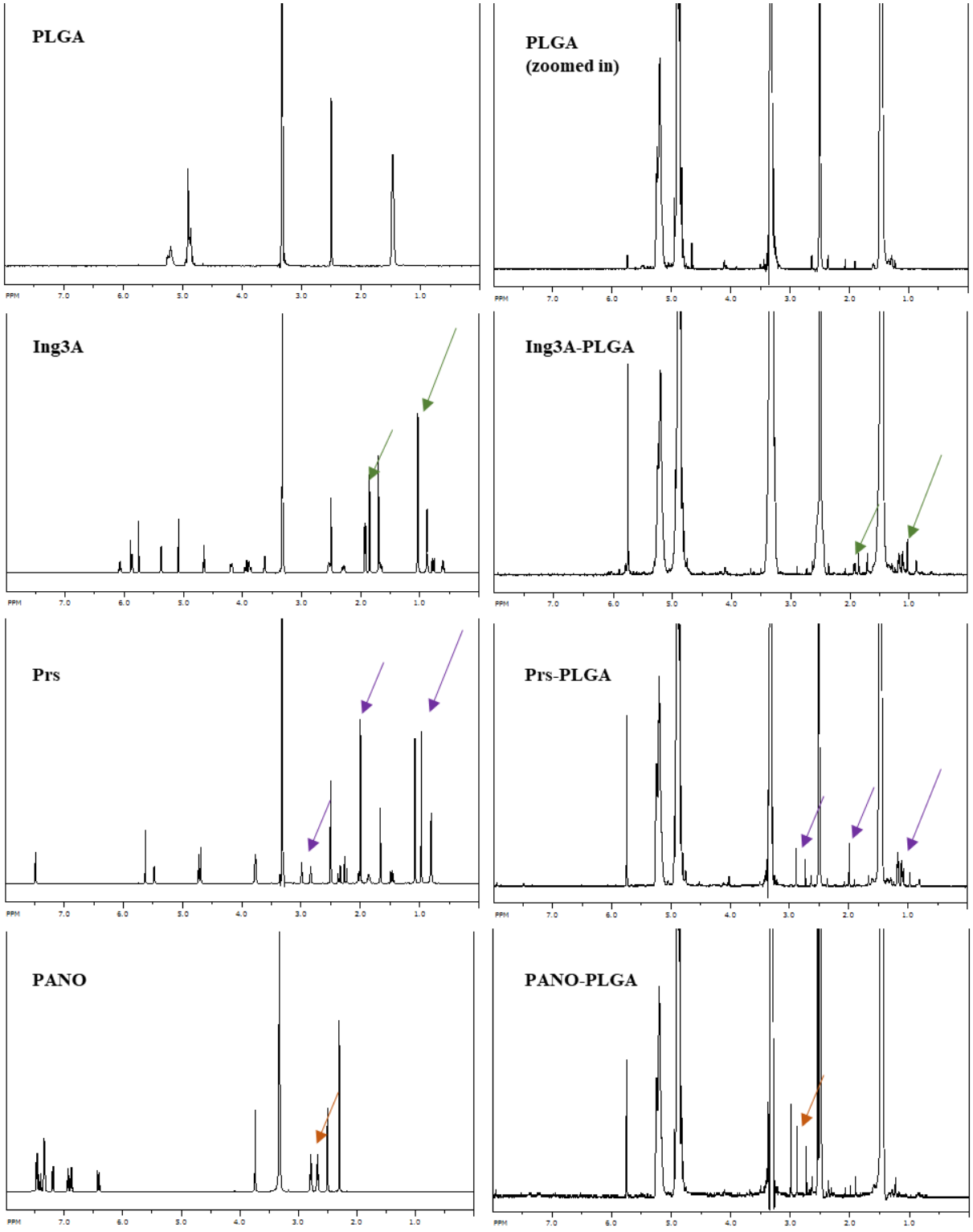

Fig. S1. H-NMR analysis of PLGA, LRA and PLGA-LRA conjugates. Arrows indicate chemical shifts from LRAs. All shifts from LRAs in the conjugates were low due to conjugation of LRA (low m.w.) to PLGA (high m.w.) at 1:1 molar ratio.

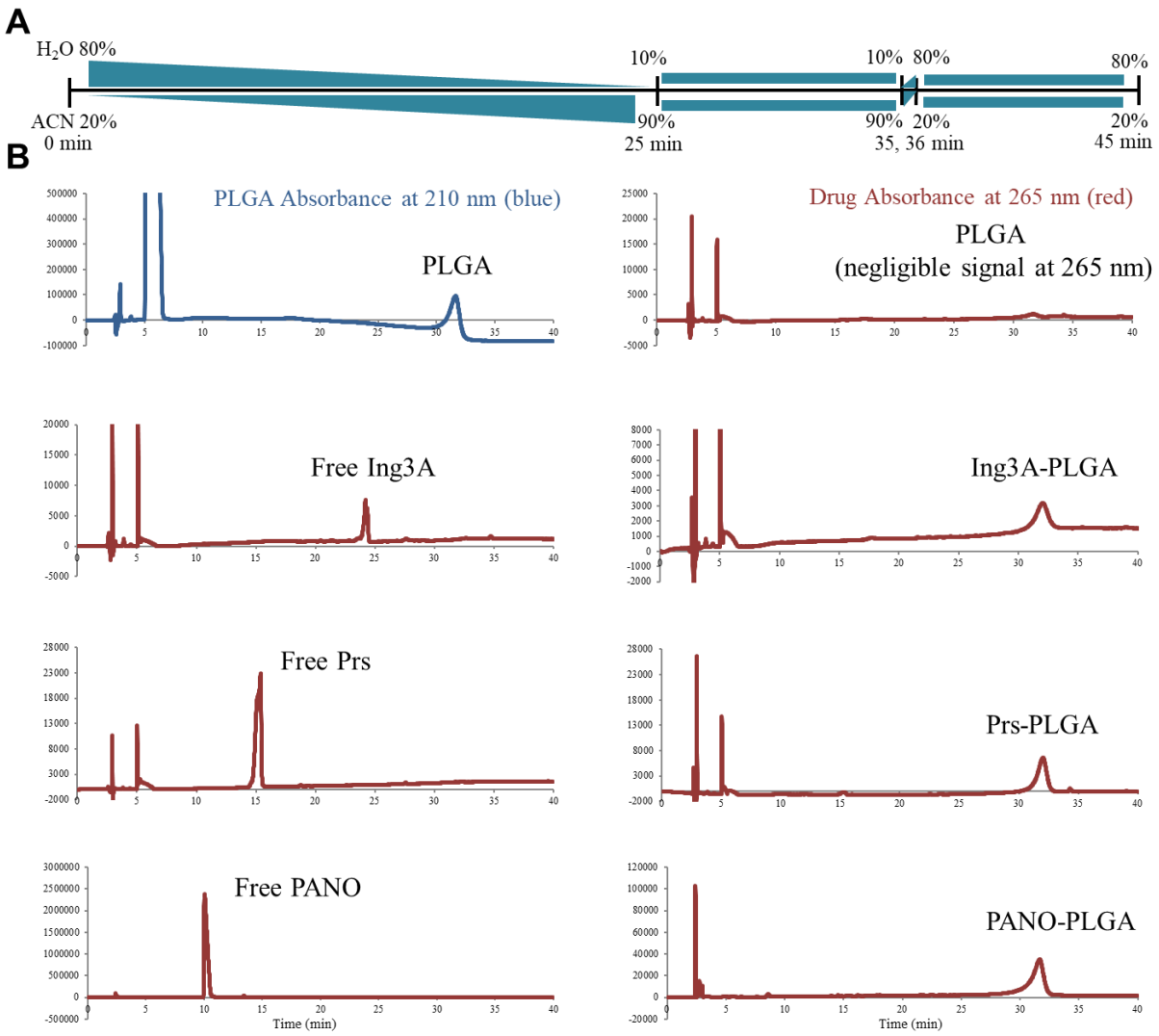

Fig. S2. HPLC analysis of PLGA-LRA conjugates. (A) Water-acetonitrile (ACN) gradient eluting method for high performance liquid chromatography (HPLC) analysis of free LRA, PLGA and PLGA-LRA conjugates. **(B)** HPLC analysis of PLGA at 210 nm (blue) or 265 nm (red) wavelength, and free LRA and PLGA-LRA conjugates at 265 nm wavelength. PLGA and PLGA-LRA conjugates were eluted at 30-35 min.

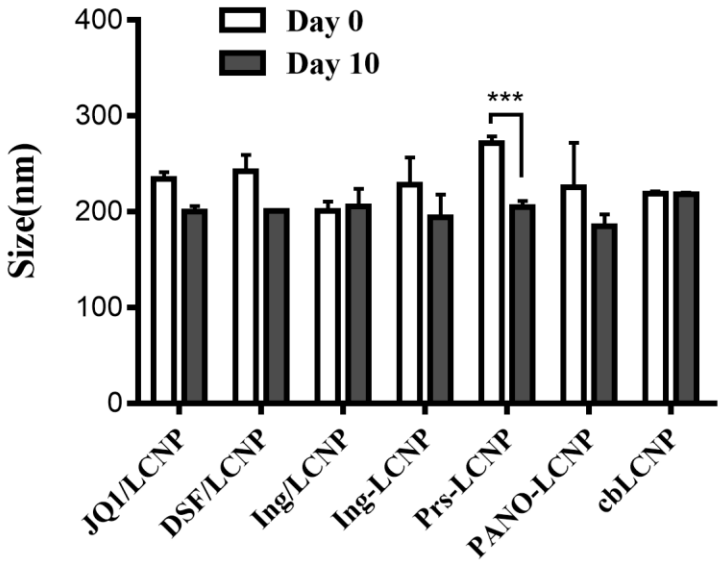

Fig. S3. Colloidal stability of LRA- loaded LCNPs. LCNPs were incubated in cell culture media at 37 °C for 10 days. Sizes were measured by DLS. Statistical significance was calculated using two-way ANOVA with Bonferroni's test. *** $p<0.0005$, otherwise not significant between day 1 and day 10. Data represent mean ± s.d.; $n = 3$.

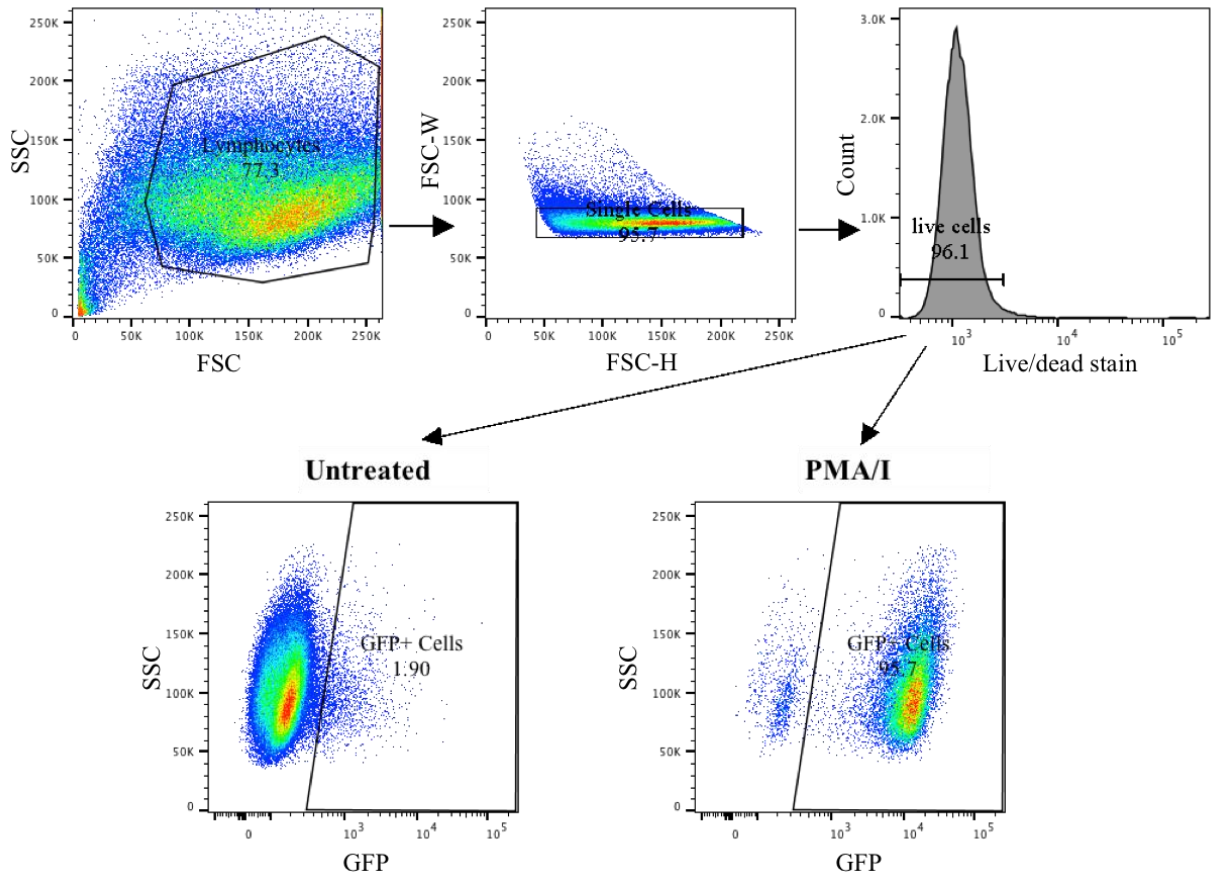

Fig. S4. Flow cytometry dot plots showing the entire gating strategy used to identify GFP$^+$ cell populations of J-Lat A1 cells. This gate strategy is applied to Fig. 2B&C, Fig. 3B, and fig. S5A&S6A.

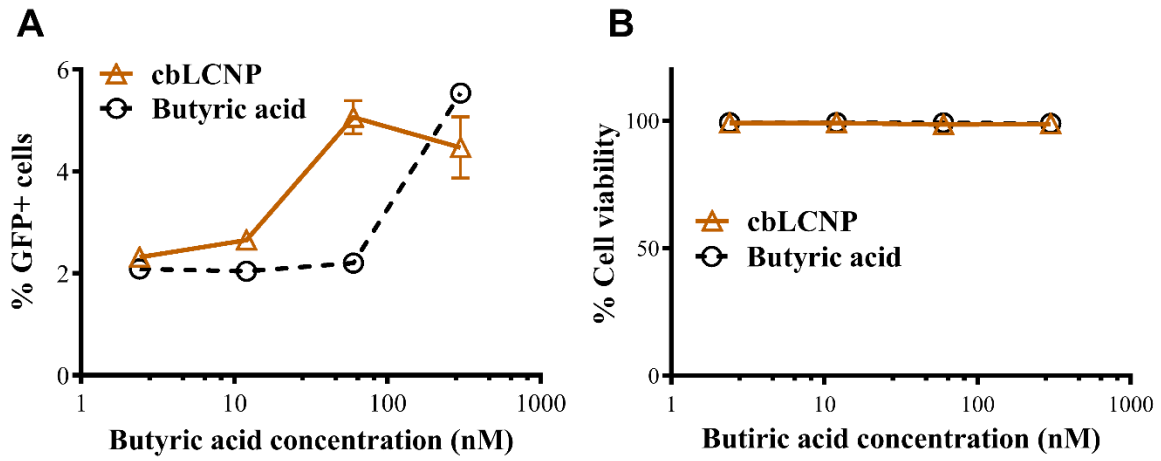

Fig. S5. In vitro dose-response HIV-1 latency reversal and cytotoxicity by free butyric acid or its prodrug inserted into LCNPs. (**A**) Dose-response curve for latent HIV reactivation (indicated as a percentage of GFP+ cells) on J-Lat A1 cells incubated with butyric acid or cbLCNPs for 20 hours. cbLCNP: LCNPs with cholesteryl butyrate inserted into the lipid layer. (**B**) Cell viability after treating with butyric acid or cbLCNPs for 20 hours. Data represent mean ± s.d.; *n* = 3.

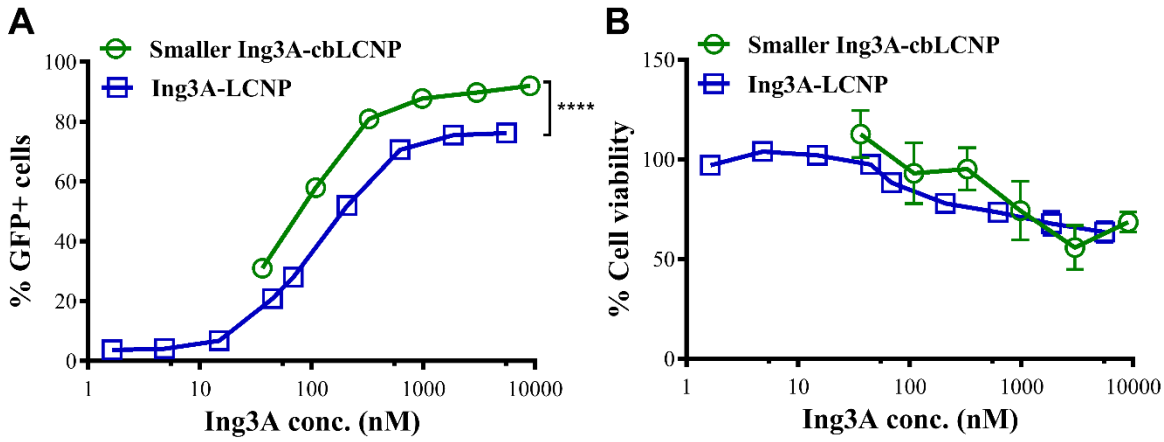

Fig. S6. In vitro dose-response HIV-1 latency reversal and cytotoxicity by smaller Ing3A-cbLCNP compared to previous Ing3A-LCNP formulation. (**A**) Dose-response curve for latent HIV reactivation (indicated as a percentage of GFP+ cells) on J-Lat A1 cells incubated with smaller Ing3A-cbLCNPs (green circle) for 20 hours. The curve from previous Ing3A-LCNPs (blue square) was included here from Fig. 2B for comparison. (**B**) Cell viability after treating with smaller Ing3A-cbLCNPs for 20 hours. The cytotoxicity curve from previous Ing3A-LCNPs was included here from Fig. 2D for comparison. Statistical analysis was performed using unpaired Student's *t* test after best-fit values from the nonlinear regression analysis. **** $p < 0.0001$. Data represent mean ± s.d.; *n* = 3.

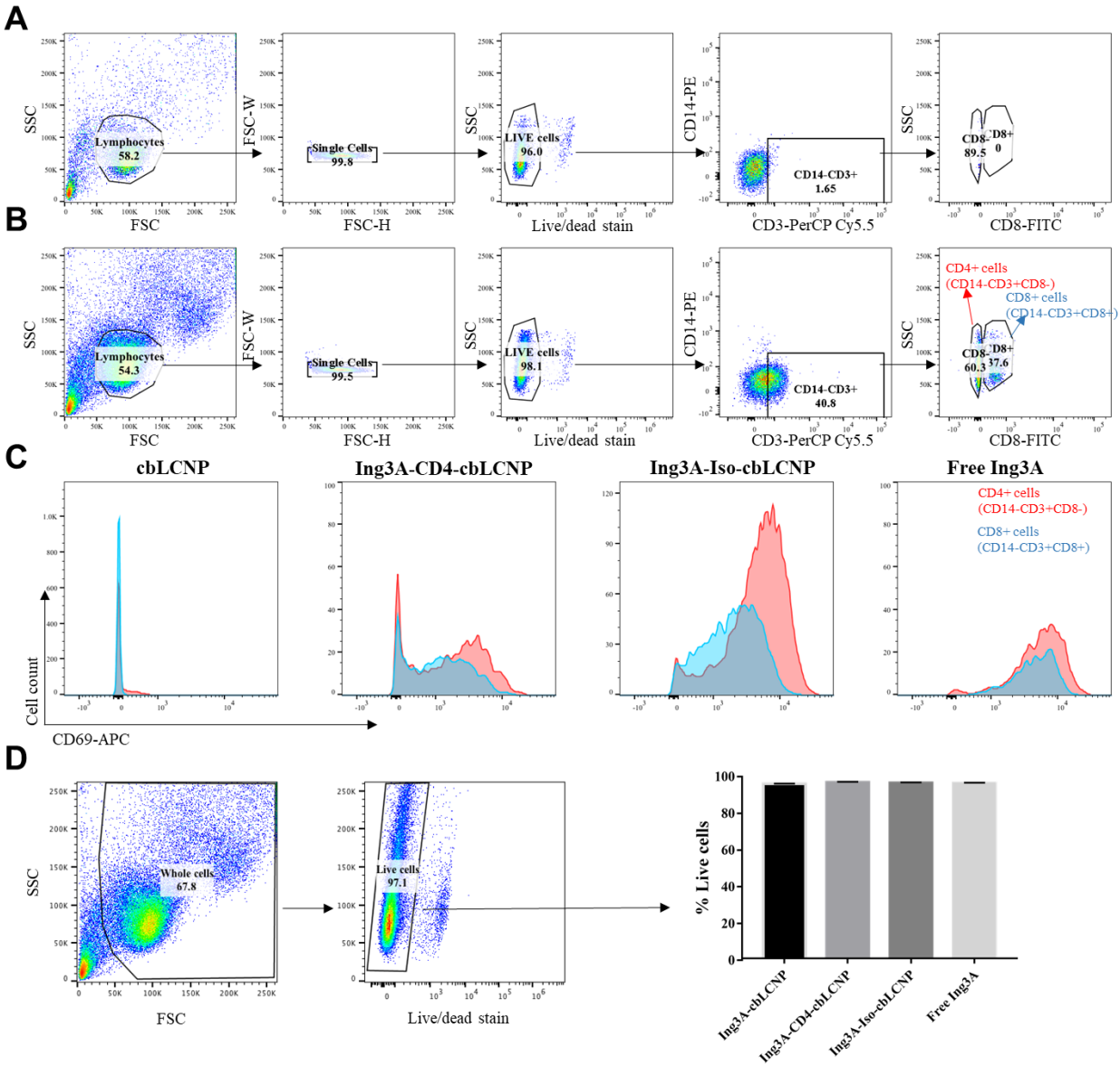

Fig. S7. Comparison of CD69 expression between CD8⁺ and CD4⁺ T cells from NHP PBMCs after treating with Ing3A formulations. (A, B) Flow cytometry dot plots showing the entire gate strategy utilized to distinguish CD4+ (CD14-CD3+CD8-) and CD8+ (CD14-CD3+CD8-) T cells in NHP PBMCs**.** Isotype control is shown in (A). We defined CD4+ T cells by CD3+CD14-CD8- because the CD4-cbLCNPs bind to CD4 and prevent binding by antibodies used for flow cytometry. **(C)** Histograms of mean fluorescence intensity of CD69 expression by the indicated CD8+ (blue) or CD4+ (red) T cell subsets in NHP PMBCs. PBMCs were treated with free Ing3A, bare LCNPs, CD4-targeted LCNPs and isotype LCNPs for 20 hours. CD69 MFI data were plotted in Fig. 4B. **(d)** Flow cytometry dot plots showing the gate strategy utilized to identify live cells from whole PBMC cells. Percentages of live cells after incubation with various Ing3A formulations are plotted in the right bar graph. Data represent mean ± s.d.; n = 3.

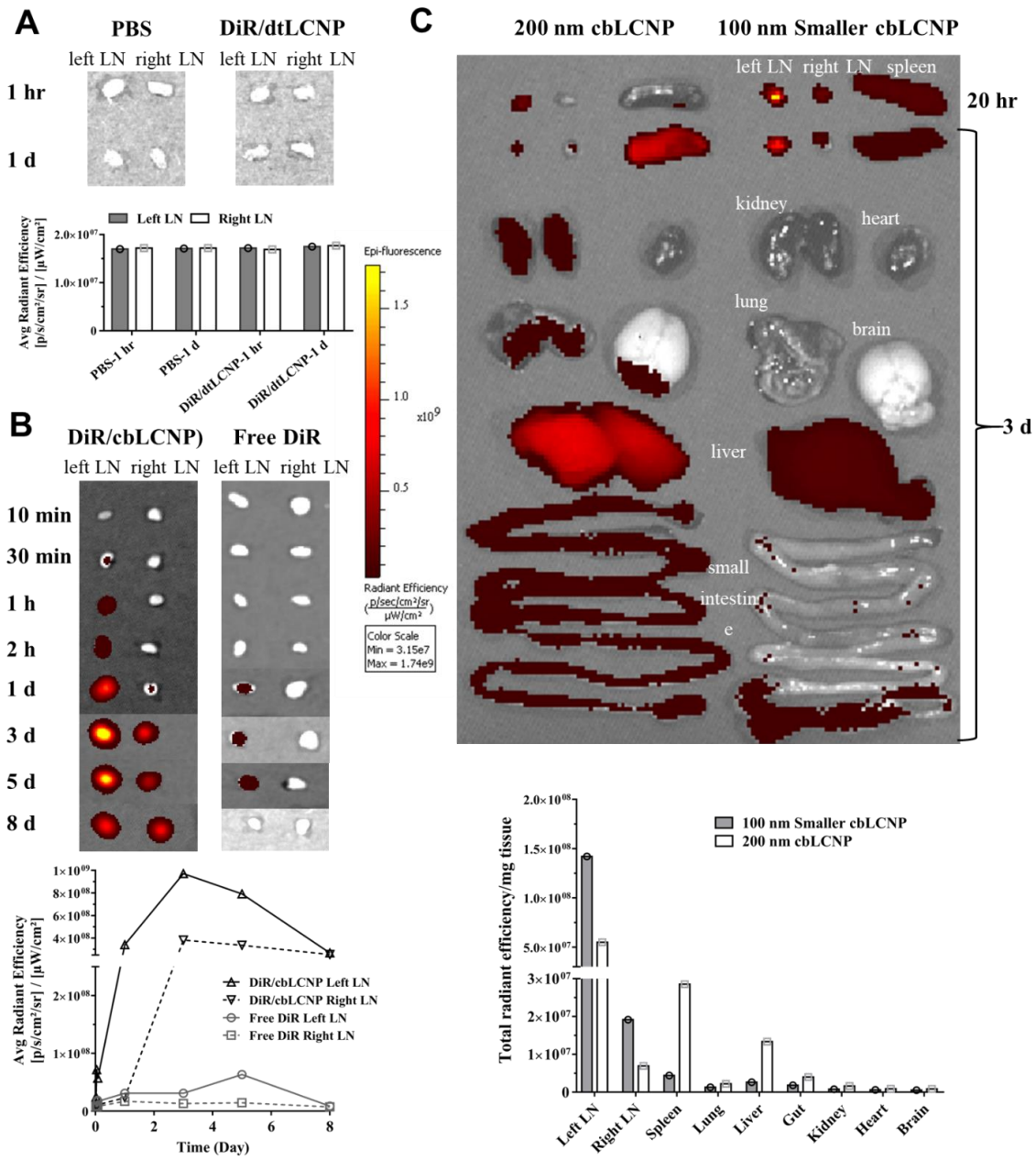

Fig. S8. Pilot mouse studies comparing biodistribution of different LCNP formulations. (A) Fluorescent images of inguinal lymph nodes (LNs) of mice after being subcutaneously injected with PBS or DiR labeled dtLCNPs (neutral LCNPs with DOTAP in the lipid bilayer, 86 μg/mL DiR) at 1 hour or 1 day. Fluorescent signals were not observed from both left and right LNs. Average radiant efficacies from those LNs were plotted below. **(B)** Fluorescent images of LNs of mice at different time points post-administration of DiR dye labeled cbLCNPs (negatively-charged LCNPs with cholesteryl butyrate inserted into the lipid bilayer) or equivalent free DiR dye (86 μg/mL DiR). Average radiant efficacies from those LNs were plotted below. **(C)** Fluorescent images of LNs and other major organs of mice after being subcutaneously injected with 200 nm or 100 nm DiR labeled cbLCNPs (25 μg/mL DiR) at 20 hours or 3 days. Total fluorescent signal normalized by tissue mass were plotted below. All the fluorescent images share the same scale bar in the middle.

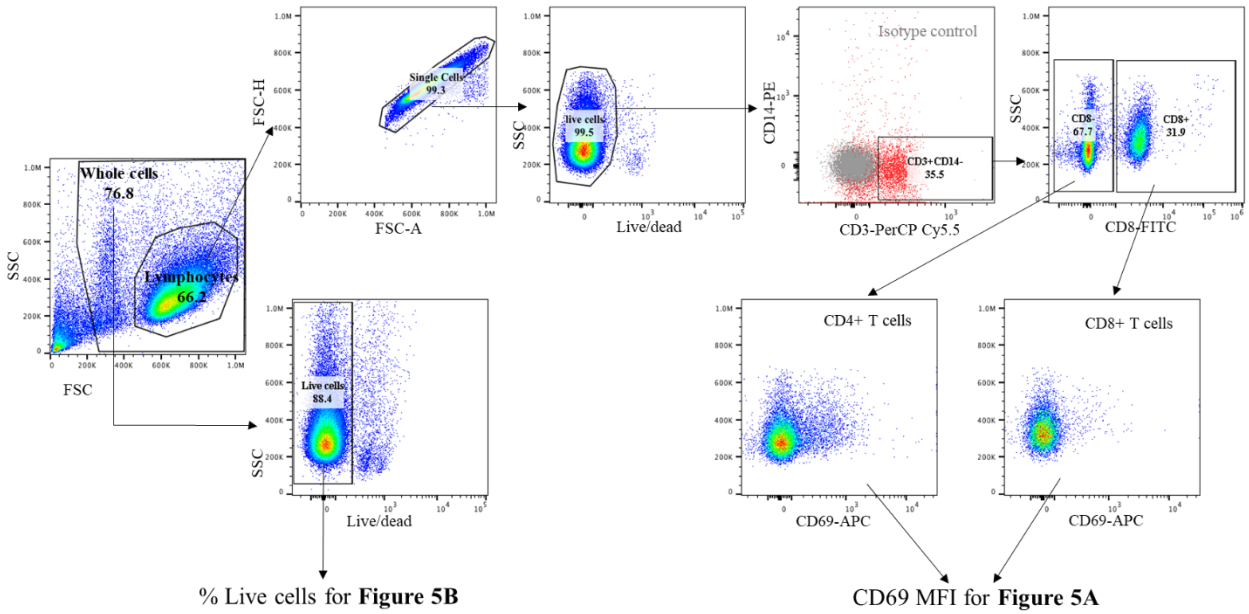

Fig. S9. Flow cytometry dot plots showing the entire gating strategy applied in Fig. 5. Percentage of live cells in Fig. 5B were gated from whole cells that include dead cells and other cell populations. Mean fluorescent intensity (MFI) of CD69 expression from distinguish CD4+ (CD14-CD3+CD8-) and CD8+ (CD14-CD3+CD8+) T cells were plotted in Fig. 5A. Fig. 5C used a similar gating strategy, except for measuring MFI of DiD fluorescent signal instead of CD69-APC. Isotype control is shown in grey.

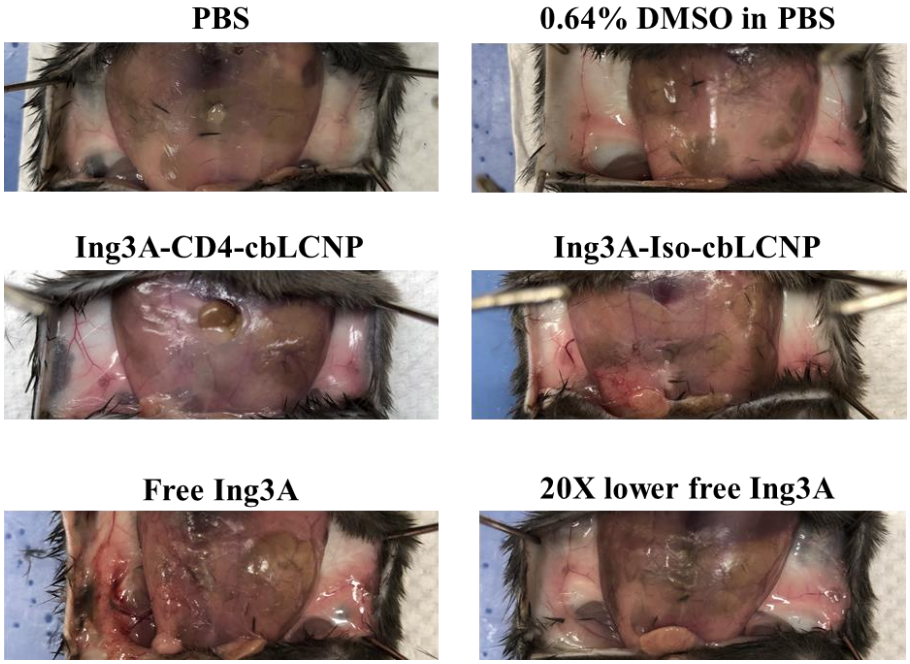

Fig. S10. Representative images of mouse subcutaneous tissues at 3 days after administration of different Ing3A formulations. Substances were injected subcutaneously into the left side flank of mice. Photo credit: Shijie Cao, Department of Bioengineering, University of Washington.

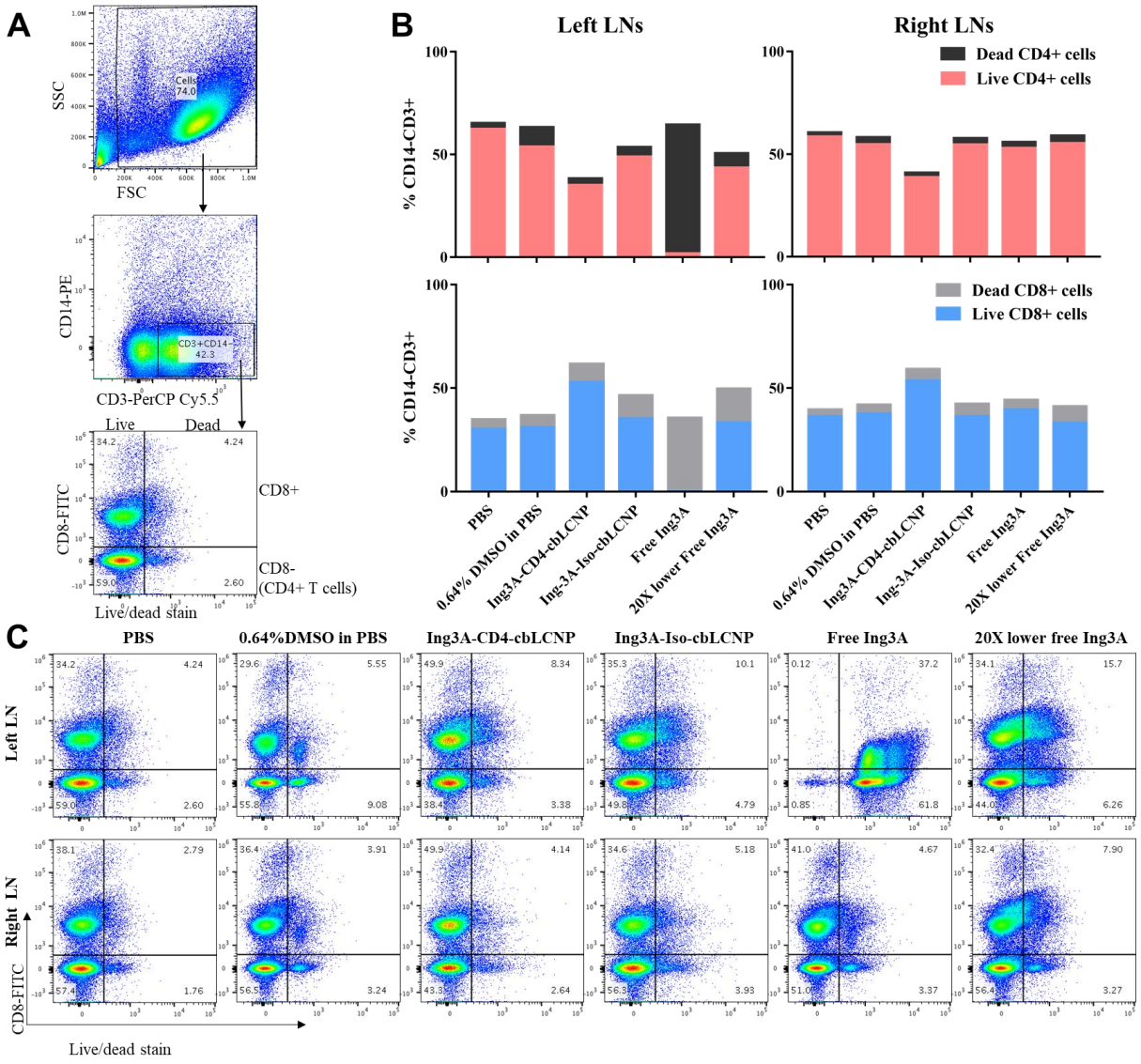

Fig. S11. Targeted LCNP-formulated Ing3A is nontoxic to CD4⁺ and CD8⁺ T cells in mouse LNs after subcutaneous dosing. (A) Flow cytometry dot plots of primary cells isolated from mice inguinal lymph nodes, showing the gating strategy applied in Fig. S11B, C. **(B)** Live or dead CD4+ (CD14-CD3+CD8-) and CD8+ (CD14-CD3+CD8+) T cells as a percentage of the CD3+CD14- parent population in mice left or right inguinal lymph nodes at 20 hours after treatments. Data represent mean. **(C)** Representative flow cytometry dot plots for Fig. S11B. *n* = 3 mice per group.

Table S1. Physicochemical properties of LCNP - formulated LRAs with unsatisfactory low drug loading.

LRAs	Prs[a]	Romidepsin	
Molecular Target	PKC	HDAC	
[b]Formulation Strategy	Single-emulsion (EtOAc)	Single-emulsion (EtOAc)	Single-emulsion (DCM)
[c]Size (d, nm)	209.0 ± 3.3	176.0 ± 2.9	234.0 ± 0.8
[c]Polydispersity Index	0.06 ± 0.01	0.06 ± 0.01	0.11 ± 0.05
Drug Input (wt%)	5	5	5
Drug Loading (wt%)	**<0.01**	**0.02 ± 0.002**	**0.18 ± 0.02**
[d]EE (%)	**<0.2**	**0.4 ± 0.2**	**3.8 ± 0.4**

[a]Data for Prs (prostratin) were from cbLCNP formulation with chol-but inserted into the lipid bilayer;
[b]LRAs were dissolved in ethyl acetate (EtOAc) or dichloromethane (DCM) with PLGA following single-emulsion evaporation method;
[c]Size and polydispersity index were measured by DLS. Data present mean ± s.d., $n = 3$.
[d]EE: encapsulation efficiency is the ratio of the actual loading (wt%) to the drug input (wt%) expressed as a percentage.

Table S2. Physicochemical properties of LCNPs made of various PLGAs.

[a]PLGA	Resomer®					Lactel®
	752H	**502H**	**503H**	**505**	**756S**	**B6013-2**
L:G ratio	72:25	50:50	50:50	50:50	72:25	75:25
Molecular Weight	4,000-15,000	7,000-17,000	24,000-38,000	54,000-69,000	76,000-115,000	~70,000-115,000[b]
End group	Acid	Acid	Acid	Ester	Ester	Ester
Transition Temperature (°C)	42-46	42-46	44-48	48-52	49-55	NA
Viscosity (dL/g, in chloroform)	0.14-0.22	0.16-0.24	0.32-0.44	0.61-0.74	0.71-1.0	0.55-0.75
[c]Size (d, nm)	194.2 ± 3.7	204.0 ± 34.6	165.9 ± 0.6	174.9 ± 2.8	181.6 ± 2.6	193.0 ± 1.9
[c]PDI	0.24 ± 0.01	0.23 ± 0.04	0.06 ± 0.05	0.08 ± 0.03	0.04 ± 0.01	0.07 ± 0.02
[c]ζ-potential (mV)	4.1 ± 0.6	8.1 ± 0.6	15.2 ± 1.7	17.3 ± 0.2	19.0 ± 0.4	9.4 ± 2.2
[d]Colloidal Stability	<1 d	<1 hr	>5 d	>5 d	>5 d	>5 d

[a]Properties of PLGA, including lactide:glycolide (L:G) ratio, molecular weight, end group, transition temperature, and viscosity were obtained from manufacturers' websites.
[b]Molecular weight of Lactel® PLGA is estimated based on its inherent viscosity using online sources.
[c]Size, PDI (polydispersity index), and ζ-potential were measured by DLS. Data present mean ± s.d.; $n = 3$.
[d]Colloidal stability is indicated as the time when the particle size changes and the PDI becomes larger than 0.3 in a physiological condition (cell culture media).

Table S3. Parameters from fitting to LRA release kinetics.

Treatment	Term	Estimate	Error	Statistic	P-Value	Release (%) at 20 hours
JQ1/LCNP	K	51.18587	3.637391	14.07214	4.32E-13	89.0646
	n	0.076936	0.017397	4.422411	0.00018	
	K0	38.59328	3.398875	11.35472	3.89E-11	
DSF/LCNP	K	43.15689	5.442451	7.92968	9.48E-08	53.9556
	n	0.270607	0.039021	6.934945	7.51E-07	
	K0	12.88075	4.74881	2.712416	0.013046	
Ing3A/LCNP	K	48.04601	7.163138	6.707397	1.23E-06	38.6922
	n	0.333127	0.049355	6.74961	1.12E-06	
	K0	-6.51646	6.101818	-1.06795	0.297665	
Ing3A-LCNP	K	7.978264	1.036291	7.698865	6.18E-08	3.9318
	n	0.584354	0.035957	16.25155	1.87E-14	
	K0	-3.23853	1.20181	-2.69471	0.012659	
Prs-LCNP	K	5.603765	0.541304	10.35235	2.49E-10	2.7266
	n	0.702044	0.02742	25.60345	6.17E-19	
	K0	-2.20247	0.738635	-2.98181	0.00648	
PANO-LCNP	K	47.76548	6.733931	7.093254	5.36E-07	43.5120
	n	0.244131	0.03581	6.8175	9.67E-07	
	K0	-2.16963	5.828599	-0.37224	0.713446	

$D(t) = Kt^n + K_0$

LRA/LCNP: LRA was physically encapsulated into LCNPs;
LRA-LCNP: LRA was chemically conjugated to the PLGA.

Table S4. Parameters from fitting to LRA dose-response curve.

Treatment	Slope	Lower Asymptote	Upper Asymptote	ED_{50} (nM)	rss
Free JQ1	-0.952364472	1.792652141	17.7039573	527.2488977	0.2392336006
JQ1/LCNP	-0.859372275	1.686678936	22.99286216	724.2970616	0.6315654068
Free DSF	-4.394655497	2.096852241	12.34579196	6018.806782	1.022873701
DSF/LCNP	-7.205209276	2.978245138	29.76341519	8494.777986	0.7526946443
Free Ing3A	-1.135179667	1.264189559	88.2731729	12.94915491	0.760276042
Ing3A/LCNP	-1.123422048	1.174486132	90.80389617	10.92800672	0.4822496735
Ing3A-LCNP	-1.246198532	2.439440274	77.57906768	116.4025408	0.9142957024
Free Prs	-1.849678762	1.888034372	84.616624	667.3110757	0.0955698905
Prs-LCNP	-1.34247879	2.983788141	100.1273641	27702.77825	0.4617669071
Free PANO	-1.683672937	2.453852081	79.20236538	22.74938412	0.8967216535
PANO-LCNP	-1.932296976	1.19373663	75.39156718	82.18765588	1.795007682

$f(x) = c + \frac{d-c}{1+e^{b(\log x - \log e)}}$

b = slope, e = ED50, c = lower asymptote, d = upper asymptote; rss, residual summary of squared error;
LRA/LCNP: LRA was physically encapsulated into LCNPs;
LRA-LCNP: LRA was chemically conjugated to the PLGA.

Table S5. Synthesis optimization for smaller LCNPs.[a]

Formulations	PLGA (mg/mL)	Lipids (mg/mL)	Organic: Aqueous Ratio	Size, Z-ave (d, nm)	Size, Number Mean (d, nm)	Polydispersity Index
Original	10	1	1 : 2	219.27	196.83	0.057
Varying PLGA Concentration	1	1	1 : 2	172.72	113.07	0.144
	5	1	1 : 2	190.57	148.53	0.11
	20	1	1 : 2	260.53	210.43	0.132
Varying Organic: Aqueous Ratio	5	1	1 : 4	158.79	99.59	0.164
	5	1	1 : 6	235.7	91.34	0.305
	10	1	1 : 2.5	193.13	158.27	0.086
	10	1	1 : 4	166.4	126.07	0.113
	10	1	1 : 6	155.63	99.38	0.186
	10	1	1 : 10	246.07	98.59	0.213
Varying Lipid Concentration	5	2	1 : 4	183.74	93.79	0.287
	10	**2**	**1 : 4**	**146.2**	**100.04**	**0.141**
	10	3	1 : 4	168.03	94.05	0.244

[a]LCNP sizes were measured by dynamic light scattering (DLS) and presented as both Z-ave and number mean here. $n = 1$.